

Impact of Surface Charge Density and Motor Force Upon Polyelectrolyte Packaging in Viral Capsids

Qianqian Cao,^{1,2,3} Michael Bachmann^{2,4,5}

¹College of Mechanical and Electrical Engineering, Jiaxing University, Jiaxing 314001, People's Republic of China

²Soft Matter Systems Research Group, Center for Simulational Physics, The University of Georgia, Athens, Georgia 30602

³Institut für Theoretische Physik, Freie Universität Berlin, Arnimallee 14, 14195 Berlin, Germany

⁴Instituto de Física, Universidade Federal de Mato Grosso, 78060-900 Cuiabá (MT), Brazil

⁵Departamento de Física, Universidade Federal de Minas Gerais, 31270-901 Belo Horizonte (MG), Brazil

Correspondence to: Q. Cao (E-mail: qqcao@mail.zjxu.edu.cn)

Received 16 September 2015; accepted 20 January 2016; published online 8 March 2016

DOI: 10.1002/polb.24019

ABSTRACT: By means of Langevin molecular dynamics simulations, we study the packaging dynamics of flexible and semiflexible polyelectrolytes in spherical cavities that resemble viral capsids. We employ a coarse-grained model of the polymer-capsid complex that allows us to perform simulations of a 900mer and investigate the influence of surface charges inside the capsid and an additional motor force, acting on the polymer in the portal region of the cavity, on the packaging process. Our results indicate that it is most efficient if surface charges are present that initially promote the formation of an

ordered surface layer inside the capsid. Once these charges are screened, the motor force pulls in the remaining part of the chain. Additionally, the simulations also demonstrate that the packaging dynamics depends on the counterion valence. © 2016 Wiley Periodicals, Inc. *J. Polym. Sci., Part B: Polym. Phys.* **2016**, *54*, 1054–1065

KEYWORDS: capsid; molecular dynamics; molecular mechanics; polyelectrolytes; stiffness

INTRODUCTION Viruses, which are among the simplest biological systems, occur in an abundant variety in nature. A single virus typically consists of a protein coating (capsid) and a genome enclosed in the capsid. The genetic material may be composed of DNA or RNA which is either single-stranded (ss) or double-stranded (ds). The capsid is assembled by concatenation of discrete protein units. Its formation may be guided in the presence or absence of the viral genome, which depends on the species of viruses and external conditions such as salt concentration. For capsid assembly processes, in which the genome does not actively participate, the viral capsids form spontaneously, and after its creation DNA or RNA molecules are packed into the empty capsid. Understanding the details of viral assembly and genome packaging is necessary for the development of antiviral drugs. This knowledge is also useful in bionanotechnology as it supports the systematic fabrication of virus-like nanocontainers.

The capsid, with typical dimensions in the range of tens of nanometers, can exhibit cylindrical, conical, or nearly spherical shapes. The spherical-like viral capsid can mathematically be described as an icosadeltahedral structure, as it features small deviations from a perfectly spherical shape.¹ Due to

recent technological advances, high-resolution information of virus structures can also be obtained experimentally.^{2–5}

The space enclosed by viral capsids is highly limited, and the successful accommodation of charged flexible and semiflexible polymers such as RNA and DNA by a spontaneous intrusion process is only possible under strict conditions typically not present in biological systems.⁶ Packaging of DNA into viral capsids and the confinement of a polyelectrolyte chain into a small space require an ordering principle that allows for efficient use of the available space. In recent years, various studies have paid particular attention to investigations of the formation of spatial conformations of polymers under geometrical confinement, for example, in association with the assembly of viruses and virus-like particles,^{7–11} confinement-influenced crystallization of polymers,^{12–14} and translocation of DNA through nanopores.^{15,16}

The spatial confinement is unfavorable because the characteristic length scale of the confined space is generally smaller than the persistence length of the chain. The dsDNA with a persistence length of about 50 nm under physiological conditions is subject to high energetic and entropic penalties when launched into a small rigid capsid. On the other hand, only the strong pressure generated by packaging a

© 2016 Wiley Periodicals, Inc.

macromolecule in confined space enables the injection mechanism that shoots viral DNA out of the capsid and into a host cell.

The packaging of many viral genomes is aided by a powerful ATP-driven motor which is part of a complex of portal protein domains. The packaging force is initially small, but then raises dramatically, because of the high internal pressure due to volume exclusion and charge effects. Consequently, this phase of genome intrusion is accompanied by a rapid decrease in the packaging rate as more segments of the DNA are inserted.¹⁷ A number of theoretical studies^{18–28} have addressed the packaging dynamics of the genome, and found good agreement with experimental findings. In these studies, the genome is fed into the capsid either at a constant rate or a constant force pulling in the chain into the capsid at its portal. In addition, sometimes a specific initial conformation of the genome is assumed and a predefined structure inside a capsid is chosen.^{29–31} Kindt et al. used Brownian dynamics to simulate the DNA packaging in a bacteriophage.¹⁸ Their results reported a spool-like structure of the DNA and revealed that the force which resists the DNA packaging process increases significantly during the final loading stage. Forrey and Muthukumar suggested that statistical mechanics, rather than molecular mechanical dynamics, should serve as the proper theoretical basis for genome packaging.²⁰ The genome packaging in viral capsids with different geometries also received theoretical attention recently.^{19,22} It was found that a flexible polymer chain is packed more rapidly into a spherical capsid but ejected more slowly than from an ellipsoidal capsid, while semiflexible chains are packed and ejected more easily in and from a spherical capsid.¹⁹ Electrostatic interaction between DNA segments²⁷ and salt concentration²⁶ can influence genome packaging and ejection as well as the possible conformations of packed DNA. For capsids with more details, various conformations of dsDNA were identified, which not only depend on the size and shape of the capsid but also on the size of the protein portal.²² It was also shown that electrostatic interactions between the capsid and the genome non-negligibly control the length and conformation of the genome.^{32,33} Furthermore, electrostatic mechanisms were found to be essential for the build-up of force by the bacteriophage T4 DNA packaging motor³⁴ and capsid assembly.³⁵ It also turned out that the topological friction for disordered, highly entangled DNA conformations and for twist knots of DNA leads to a significant slowdown in DNA ejection.³⁶ The kind of the knot but not the pressure of confinement controls primarily the ejection rate, and the flexibility of the polymer is not important in determining the rate of ejection for tightly confined knots.³⁷

The surface of viral capsids includes complex local structures of protein units such as peptide arms. Additionally, various competing interactions determine the structural behavior of the genome inside the capsid. In particular, the electrostatic interaction profoundly affects the conformation and packaging dynamics of the genome. However, in previous computational studies much less attention was paid to how the local

details of the capsid and the electrostatic interaction between the capsid and the genome influence the packaging dynamics in viruses. Most of these studies mainly focus on the packaging dynamics and evolving structure with the help of motor force, regardless of the details of the capsid. Experimentally, it is also difficult to determine the role of the surface properties of the capsid in the packaging process and its effect on the conformation of the tightly packed DNA.

Most recent computational studies that address the packaging and ejection dynamics of viral genomes employ simplified coarse-grained models. There are two main reasons as following: First, viral systems typically contain a large number of atoms. For example, all-atom molecular dynamics simulations of the satellite tobacco mosaic virus with a small diameter of about 17 nm requires up to 1 million atoms to analyze its structural stability.³⁸ If one wants to address the packaging dynamics of viral genomes, a larger system is doubtless needed. Second, the packaging or ejection time-scale spans from milliseconds to minutes. As far as the present computational power is concerned, it is virtually impossible to carry out such time-consuming all-atom molecular dynamics simulations for such large systems. Therefore, it is necessary to adopt a coarse-graining strategy for the all-atom viral systems. In general, the coarse-grained capsid models are represented as either specific shapes for real viruses^{21,31} or perfect geometrical shapes such as spherical and elliptic,^{19,39} and most simulations were conducted using implicit ion and solvent models. In this work, a generic virus model with ideal spherical shape is employed. The present study does not specifically aim at explaining a single type of virus. Based on our coarse-grained model, we investigate general packaging characteristics of a polyelectrolyte into a spherical cavity representing a virus-like system. In our simulations, the polyelectrolyte is packed into an oppositely charged capsid by applying an effective motor force at the capsid portal and the effect of the capsid charges upon packaging dynamics and conformational properties of the polyelectrolyte is explicitly investigated. In the simplified model, we consider a charged cavity that can be regarded as a capsid with net positive charges. This study extends our recent analysis of the spontaneous intrusion of a polyelectrolyte into a charged cavity if no motor force is present.⁷

MODEL AND SIMULATION METHOD

We employ a coarse-grained bead-spring model to represent the linear cationic (negatively charged) polyelectrolyte. Coarse-grained models of polymer systems have turned out to be particularly beneficial for a systematic analysis of structural properties under thermal conditions.⁴⁰ In our study, the chain is composed of $N_p = 900$ beads with diameter σ . The viral capsid is modeled as a spherical shell of thickness 3σ . The cavity shell, represented by a double-layered wall with surface particle density $\rho_s = \sigma^{-2}$, is permeable for counterions, but cannot be penetrated by the polyelectrolyte. The choice of ρ_s corresponds to an impermeable surface,⁴¹ which can prevent leakage of the packed chain.

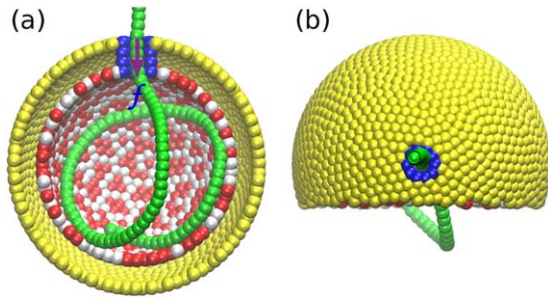


FIGURE 1 Typical snapshot of our model system of a viral capsid and a polyelectrolyte intruding into it through a portal tube. The chain is packed into the capsid with the aid of surface charges on the interior shell with charge density α and the motor force f . (a) and (b) represent a cross section of the capsid in side and top view, respectively. Counterions are not shown. Color scheme: outer shell (yellow), portal (blue), neutral (white), and charged beads (red) in inner shell, polyelectrolyte chain (green). [Color figure can be viewed in the online issue, which is available at wileyonlinelibrary.com.]

The outer wall consists of neutral particles. Positively charged particles are uniformly distributed inside the inner wall. Denoting by N_c and N_i the number of charged particles and those of all particles located in the inner wall, respectively, we introduce the ratio $\alpha = N_c/N_i$ as the internal surface charge density. In independent simulations of different capsid parameter settings, values of the surface charge density are varied in the interval $\alpha \in [0, 1]$. The chain is driven into the cavity through a tube of radius $R_t = 1.5\sigma$. We perform independent simulations for different values of the cavity radius $R \in (7\sigma, 15\sigma)$. Note that the shell thickness is not included in R . The model system is depicted in Figure 1.

The short-range excluded volume interactions between particles are modeled by the pairwise Lennard–Jones (LJ) potential

$$U_{LJ}(r) = \begin{cases} 4\epsilon_{LJ} \left[(\sigma/r)^{12} - (\sigma/r)^6 - (\sigma/r_c)^{12} + (\sigma/r_c)^6 \right], & r < r_c, \\ 0, & r \geq r_c, \end{cases} \quad (1)$$

where the potential strength is set to $\epsilon_{LJ} = k_B T$; k_B is the Boltzmann constant, and T is the system temperature. The LJ potential is truncated and shifted at a cutoff distance of $r_c = 2^{1/6}\sigma$. The shell particles, whose locations are fixed, do not interact with each other. Neighboring monomers are linked by a finitely extensible nonlinear elastic (FENE) potential with a maximum bond length $l_{\max} = 1.5\sigma$ and a spring constant $k_b = 30\epsilon_{LJ}/\sigma^2$,⁴²

$$U_b(l) = \begin{cases} -(k_b l_{\max}^2/2) \ln(1 - l^2/l_{\max}^2), & l < l_{\max}, \\ \infty, & l \geq l_{\max}. \end{cases} \quad (2)$$

The bending rigidity of the chain is modeled by using a harmonic bending potential

$$U_a(\theta) = k_\theta (\theta - \theta_0)^2, \quad (3)$$

where k_θ is the bending stiffness, and the equilibrium bond angle θ_0 is set to 180° . The potential parameter is chosen as $k_\theta = 0$ (for a flexible chain) and $k_\theta = 100k_\theta^*$ (for a semiflexible chain). Here we have introduced the bending energy unit $k_\theta^* = \epsilon_{LJ}/[\text{rad}^2]$. By assuming the polyelectrolyte behaves like a wormlike chain, we use the simple formula $l_p = 2k_\theta l_0/k_B T$ to estimate the persistence length of the semiflexible chain, where l_0 is the equilibrium bond length. For our model parameters, $l_0 \approx 1\sigma$. The estimated persistence length is $l_p \approx 200\sigma$. We use the Coulomb potential to model electrostatic interactions between charged particles:

$$U_e(r) = k_B T Z_i Z_j \frac{\lambda_B}{r}, \quad (4)$$

where the Bjerrum length $\lambda_B = e^2/(4\pi\epsilon_0\epsilon_r k_B T)$ is set to σ ; ϵ_0 and ϵ_r are the vacuum permittivity and the dielectric constant of solvent. The long-range part is calculated by means of the particle–particle/particle–mesh (PPPM) algorithm.⁴³ For water at room temperature, λ_B is approximately 0.7 nm .

The motor that drives the packaging of DNA in real viruses has a complex structure. Here, we simply introduce the net effect by applying a radial force f to the portion of DNA that occupies the region of the tube.

The Large-scale Atomic/Molecular Massively Parallel Simulator (LAMMPS)⁴⁴ was used to perform simulations in an NVT ensemble with periodic boundary conditions. The system is kept at constant room temperature ($T = 300\text{K}$) during the simulation by coupling the system to a Langevin thermostat,⁴⁵

$$m \frac{d\mathbf{v}_i(t)}{dt} = \mathbf{F}_i - \gamma m \mathbf{v}_i(t) + \mathbf{F}_i^r(t), \quad (5)$$

where \mathbf{F}_i is the total deterministic force of all particles interacting with particle i . The friction coefficient γ is used to control the relaxation rate at the given temperature and is related to the viscosity of the solvent. The value of the stochastic force \mathbf{F}_i^r is sampled from the Gaussian distribution

$$\begin{aligned} \langle \mathbf{F}_i^r(t) \rangle &= 0, \\ \langle \mathbf{F}_i^r(t) \cdot \mathbf{F}_j^r(t') \rangle &= 6m\gamma k_B T \delta_{ij} \delta(t-t'), \end{aligned} \quad (6)$$

where $\langle \dots \rangle$ denotes the ensemble average of the expression enclosed; γ is set to $1.0 \tau^{-1}$. We explicitly include counterions dissociated from the polyelectrolyte and the inner shell. Initially, the counterions are randomly dispersed within the box, and one end of the frozen polyelectrolyte is threaded through the portal tube and located inside the capsid. After a sufficiently long simulation, the distribution of counterions reaches equilibrium during which some counterions are bound to the chain. Then, the chain is unfixed and the packaging process starts. The entire system is enclosed in a cubic simulation box of edge length $L = 960\sigma$.

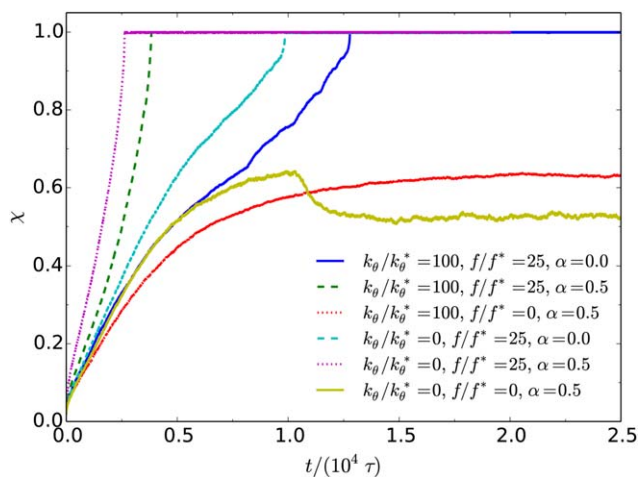


FIGURE 2 Time evolution of the packaging fraction χ of flexible ($k_\theta/k_\theta^*=0$) and semiflexible chains ($k_\theta/k_\theta^*=100$) in a capsid with radius $R = 10\sigma$. For both types of polyelectrolytes, three simulations (including $\alpha = 0$ and $f = 25f^*$, $\alpha = 0.5$ and $f = 25f^*$, $\alpha = 0.5$ and $f = 0$) were performed. [Color figure can be viewed in the online issue, which is available at wileyonlinelibrary.com.]

In our study, the LJ parameters ϵ_{LJ} , σ , and bead mass m are chosen as the basic units, leading to the corresponding time unit $\tau = (m\sigma^2/\epsilon_{LJ})^{1/2}$ and force unit $f^* = \epsilon_{LJ}/\sigma$. When the coarse-grained chain is mapped to a realistic polyelectrolyte, such as ssDNA, the resulting time and force units are $\tau \approx 20$ ps and $f^* \approx 6$ pN.

RESULTS AND DISCUSSION

In order to understand how surface charge density α , motor force f , and chain stiffness k_θ influence the packaging process of the polyelectrolyte, we show in Figure 2 the time evolution of the packaging fraction χ in the presence or absence of surface charges and motor force for flexible ($k_\theta/k_\theta^*=0$) and semiflexible chains ($k_\theta/k_\theta^*=100$). The packaging fraction is defined as the ratio of the number of monomers located inside the capsid and the total number of monomers of the polymer chain N_p .

In this case, the capsid radius R was chosen to be 10σ , which makes a tight packaging of the polyelectrolyte inside the cavity possible and allows for a comparative study of the effects upon variation of model parameters sets. In the presence of surface charges ($\alpha = 0.5$) and added motor force ($f/f^*=25$), the chain enters the cavity rapidly. The flexible chain has a slightly shorter packaging time than the semiflexible polyelectrolyte.

If no surface charges are present inside the capsid ($\alpha = 0$), but the motor is active, the overall packaging time is larger than in the previous case, which is not surprising. More interesting is that the packaging of the semiflexible chain takes substantially longer than for the flexible chain as it includes pauses that are necessary to readjust the monomer arrangement inside the capsid to make space for an additional chain segment to be pulled inside.

In coincidence with our previously found results for a much smaller system, the surface charge density of $\alpha = 0.5$ is not sufficient to let the chain intrude into the capsid spontaneously if there is no portal motor ($f = 0$).⁷ Whereas the semiflexible chain intrudes partially and then the process slows down, a larger part of the flexible chain can intrude initially, but if the internal pressure mounts beyond a threshold value, the flexible chain is partially ejected. The remaining portion of the polyelectrolyte inside the cavity is smaller than in the corresponding semiflexible-polymer case. This “springlike release”⁴⁶ of the flexible chain was not observed for small chains.⁷

The packaging speed or rate is shown for the same scenarios in Figure 3. It is defined as the number of monomers packaged into the cavity per unit simulation time τ and corresponds to the derivative of the packaging fraction (see Fig. 2) with respect to time. In the initial phase, the packaging rate is high, because the first monomers find unrivaled space in the capsid and either motor force or surface charge support quick intrusion. However, this period is very short and it is followed by a significant drop when rearrangement of monomers inside the capsid becomes necessary. For both, flexible and semiflexible polymers, packaging proceeds at a constant rate, before it speeds up again dramatically. This can clearly be attributed to the effect of the motor force that pulls the tail of the chain inside. The short tail exhibits less backward motion, and its fluctuation originating from random thermal motion of solvent molecules is remarkably weakened. This results in higher packaging rate in the final phase of the packaging process.

If no surface charges are present ($\alpha = 0$), it takes significantly longer to insert the chain by the rather weak motor force only. It is revealing to see that if no motor force is present, the chain cannot entirely be accommodated and in

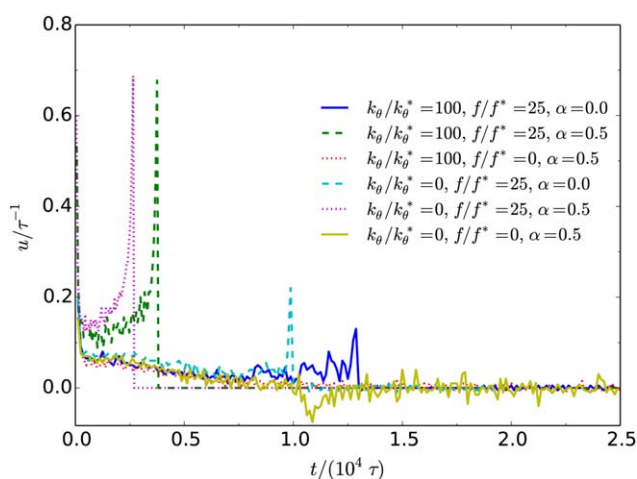


FIGURE 3 Packaging rate of flexible and semiflexible polyelectrolytes for the same capsid parameter settings as in Figure 2. [Color figure can be viewed in the online issue, which is available at wileyonlinelibrary.com.]

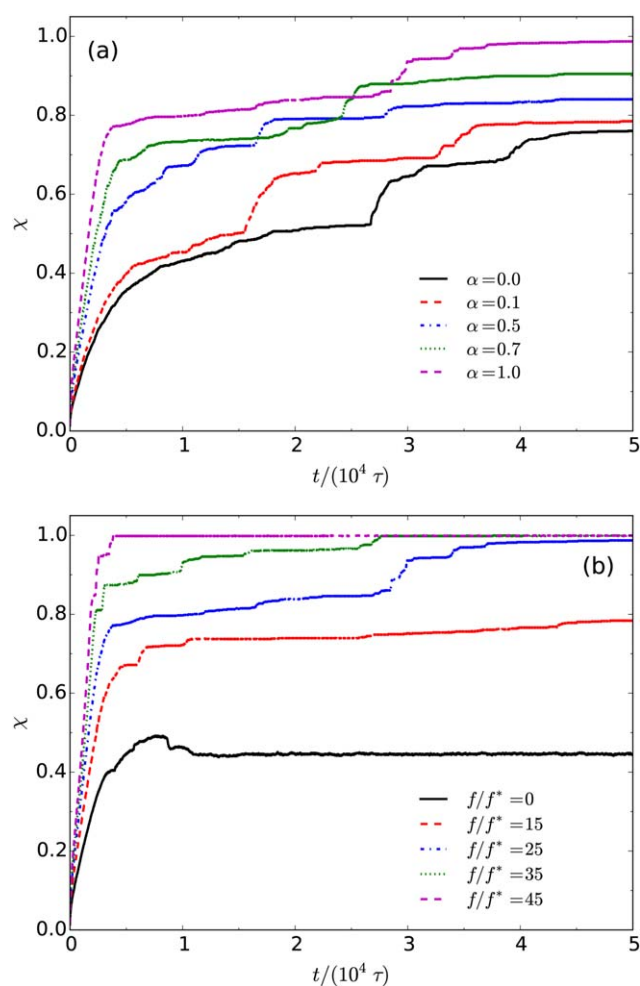


FIGURE 4 Time dependence of the packaging fraction χ of semiflexible chains at (a) $f = 25f^*$ for various surface charge fractions, and (b) $\alpha = 1$ for different values of motor forces f . The cavity radius is fixed at $R = 7.07\sigma$. [Color figure can be viewed in the online issue, which is available at wileyonlinelibrary.com.]

the case of the flexible polymer, part of the chain is released off the portal again (negative speed).

In Figure 4(a), we have plotted the packaging fraction of semiflexible chains as a function of time for various surface charge fractions ranging from $\alpha = 0$ (neutral shell) to $\alpha = 1$ (fully charged) in a cavity with radius $R = 7.07\sigma$.¹ For $R = 7.07\sigma$ and $\alpha = 1$, the total number of cavity charges is equal to that of a capsid with radius $R = 10\sigma$ at $\alpha = 0.5$. Initially, while the packaging rate largely depends on α , regular packaging dynamics are observed. After some time, the number of packed monomers saturates and reordering processes inside the capsid are necessary to prepare the electrostatic and spatial conditions that allow to pull in further monomers. These pauses are clearly visible in all curves and the reasons have been discussed in detail previously.⁷ After the rearrangement is accomplished, packaging dynamics speeds up again until further alignment becomes necessary. The reason for the pauses are consistent with the work of Forrey

and Muthukumar.²⁰ Experimentally, Smith et al. assume that pauses are a result of choppiness of the molecular motor.² However, no pauses appear in the initial stage, supporting that pauses are induced by internal chain relaxation at higher packaging densities.

Although the results show that electrostatic interaction between the polyelectrolyte and the surface charges inside the capsid is an essential driving force for the intrusion of the polymer into the cavity, it is not sufficient to achieve sufficiently tight packing inside small capsids. However, surface charges play a critical role in controlling the internal configuration of the polyelectrolyte confined in the capsid, but as more monomers are inserted into the cavity, the effect of the attractive surface charges is largely screened and their potential as an effective driving force for polyelectrolyte intrusion are reduced.

Under these conditions, an additional force is necessary for the insertion of the remaining monomers during the final stage of packaging, which can only be provided optimally by an active motor. The effect of motor support is obvious from Figure 4(b), where the packaging dynamics of a semiflexible polymer into a capsid with $R = 7.07\sigma$ and $\alpha = 1$ is shown for various values of the motor force. The results are compared with the purely electrostatic capsid without motor, that is, $f = 0$, in which case the semiflexible chain can only be partially accommodated and experiences a spring-like release. As expected, the motor supports and accelerates the polyelectrolyte intrusion initially, but it requires a minimum threshold value of the magnitude of the motor force in order to locate all monomers inside the capsid. Otherwise, the packaging is terminated if the internal pressure inside the capsid balances the pressure generated by the motor. In these cases, the semiflexible polymer forms only a single surface layer inside the cavity that partially screens the attractive surface charges. At this moment the motor would have to kick in to push further monomers through the portal into the capsid. If the motor is too weak, the part of the chain that is not pulled into the cavity wraps around and adheres to the outside shell. The process stops and polyelectrolyte inclusion remains incomplete.

We summarize quantitative results in Table 1. These data correspond to the plots in Figure 4. Figure 4 does not show the entire packaging process until equilibrium is reached. In some cases, much longer simulations would need to be performed to end up in an equilibrium state. The intrusion processes is entirely successful within the simulation period

TABLE 1 Packaging Fraction at the Equilibrium State

| α | 0 | 0.1 | 0.5 | 0.7 | 1 |
|----------|------|------|------|-----|----|
| χ | 0.79 | 0.83 | 0.91 | 1 | 1 |
| f/f^* | 0 | 15 | 25 | 35 | 45 |
| χ | 0.45 | 0.84 | 1 | 1 | 1 |

The simulation parameters correspond to Figure 4.

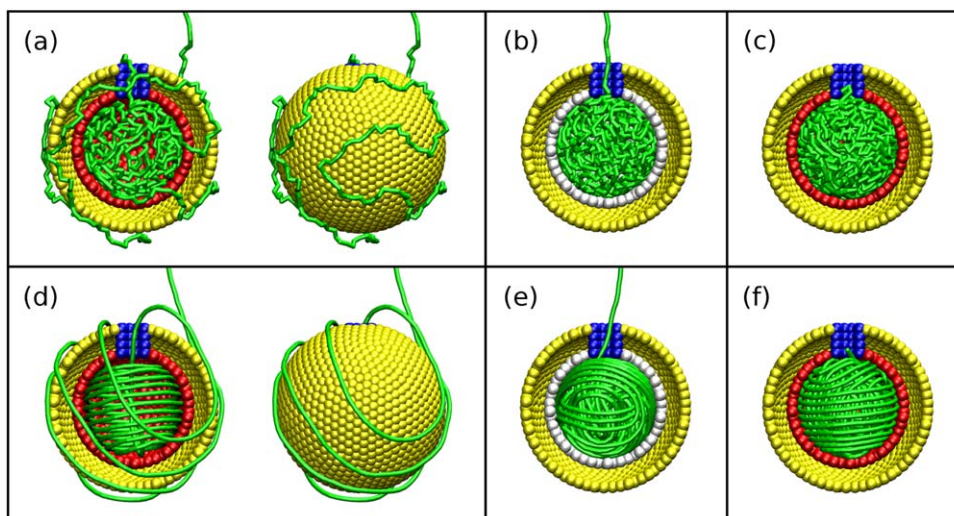


FIGURE 5 Comparison of polyelectrolyte conformations for a flexible [(a–c)] and a semiflexible polyelectrolyte [(d–f)] with 900 monomers at some time after the begin of the intrusion process for various capsid parameter settings. The radius is $R = 7.07\sigma$ and the surface charge densities α and motor forces f are (a) $\alpha = 1$, $f = 0$, (b) $\alpha = 0$, $f = 25f^*$, (c) $\alpha = 1$, $f = 25f^*$ for the flexible chain; (d) $\alpha = 1$, $f = 0$, (e) $\alpha = 0$, $f = 45f^*$, (f) $\alpha = 1$, $f = 45f^*$ for the semiflexible chain. These snapshots clearly show that only the combination of sufficiently large surface charge density and motor force enables a timely insertion of the polyelectrolyte into the capsid. [Color figure can be viewed in the online issue, which is available at wileyonlinelibrary.com.]

for high surface charge densities or large motor forces. When α is lower than 0.7 at $f = 25f^*$ or f is below $25f^*$ for the fully charged capsid, the polyelectrolyte cannot be packaged completely.

Figure 5 shows typical snapshots of the system with capsid radius $R = 7.07\sigma$ and different values of surface charge density α and motor force f for a flexible and a semiflexible 900mer at a late stage of the intrusion process. Generally, the intruded part of the flexible chain possesses a disordered, but densely packed conformation [Fig. 5(a–c)]. Since bending does not cost energy, space occupation is optimized at the expense of order.

The semiflexible polymer is forced to form much more ordered conformations. It is assumed that the minimization of bending energy of the chain results in the ordered configuration. The experiments also partly support well-ordered structures due to energy minimization.^{3,4} Bending of the chain inside the confined space of the cavity is inevitable. Therefore, the polyelectrolyte develops a spool-like structure, which is characteristic for all scenarios considered. The first monomers that intrude into the capsid are attracted by the opposite surface charges and form “hoops” that align next to each other, first with larger diameter in the equator region, then with decreasing circumference, which costs extra energy. For the surface-adsorbed layer, the net attraction by the surface charges is larger than the local repulsion by the like charges of the monomers located next to each other. After the inner surface layer is completed, spools with larger and larger curvature, assembling inner but less ordered layers, must be formed. Due to screening of the surface charges and increasing strain on the chain, the intrusion process terminates if no portal motor is present or if it is too

weak. Only for sufficiently large motor power, the process of polyelectrolyte insertion can be successfully completed, although it is accompanied by pauses as mentioned earlier. In these periods, the intruded part of the polyelectrolyte reorients itself inside the capsid. The dynamics of such a process and the structural reorientations of the polyelectrolyte have been discussed recently for spontaneous intrusion into a charged capsid without motor force.⁷

The comparison of the figures for the semiflexible polymer supports our claim that initially the surface charges of the interior shell are responsible for a preordering of the polyelectrolyte structure inside capsid by forming a surface layer. This is followed by the arrangement of additional spools with larger curvature, which requires motor assistance. Only in the case of nonzero surface charge density and motor force, the polyelectrolyte can be completely accommodated inside the capsid.

The layered assembly of semiflexible polyelectrolyte conformations in the cavity is clearly confirmed when analyzing the shape of the radial density profiles of the monomers and counterions, measured from the center of the cavity with radius $R = 7.07\sigma$. These profiles are likewise plotted in Figure 6(a) and (b) for a flexible ($k_\theta = 0$) and in Figure 6(c) and (d) for a semiflexible polymer ($k_\theta = 100k_\theta^*$) in a motor-equipped cavity ($f > 0$) without or with surface charges, that is, $\alpha = 0$ and $\alpha = 1$, respectively. Parameter values were chosen in a way that in all cases the chain could be entirely packaged into the cavity.

Not surprisingly, in all cases, the formation of a surface layer near the inner shell of the capsid is clearly signaled by a pronounced peak at about $r = 6.2\sigma$ and a second layer at r

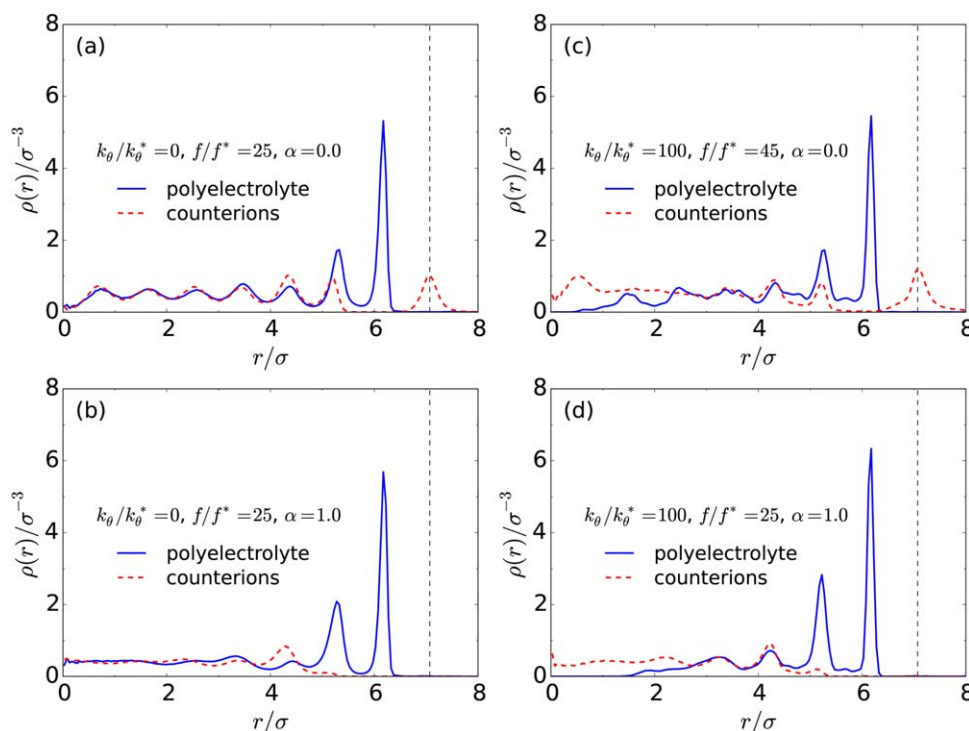


FIGURE 6 Radial density profiles of monomers and their positively charged counterions as a function of the distance from the center of the cavity with radius $R = 7.07\sigma$. The vertical line represents the location of the inner shell. No negative counterions intrude into the cavity. [Color figure can be viewed in the online issue, which is available at wileyonlinelibrary.com.]

$\approx 5.3\sigma$ can be identified accordingly. If no surface charges are present, the flexible-chain structures exhibit less pronounced radial order. In this case, high-order layers are greatly suppressed and closing in to the center of the cavity, the monomer distribution becomes almost uniform. This is very similar for the flexible chain that experiences a charged surface. In this case, the first three layers are pronounced, but closer to the center the effect of the surface charges diminishes due to screening by the outer monomer layers. In both scenarios, the applied force enables complete packaging, but it does not induce radial order. It is worth emphasizing that our simulations support the bimodal shape (two distinct peaks) of radial density profiles of RNA obtained in experiments for the flock house virus⁴⁷ and previous simulation studies of the pariacoto virus.³¹

This is completely different for the semiflexible chain. Conformations are widely arranged in layered shells, with higher density toward the inner capsid shell if it is charged. In the absence of the motor force, the monomers are only located near the charged shell regardless of how flexible or stiff the chain is, as we have found previously.⁷

If the inner shell is charged, no positive counterions are found near it. For neutral cavities, the density of counterions shows a peak at the location of the shell. The counterions are depleted in the region close to the first peak of monomer density due to compact packaging of monomers. The charges in the compact surface layer of monomers are counterbalanced by the charges of the shell for the charged cavity and

by counterions near the shell for the neutral cavity. The net charge disappears in the central region of the cavity in the case of flexible chain, but there exists a high net charge density if the chain is semiflexible [see Fig. 6(c,d)]. In general, free diffusion of counterions towards the center entails a high net charge. The higher inhomogeneity in the distribution of monomers of the semiflexible chain in the central region also leads to the higher net charge.

Compared with the case with the cavity radius of $R = 7.07\sigma$, the monomers in the larger cavity $R = 10\sigma$ mainly assemble near the shell because of the larger surface area. This is shown in Figure 7. Especially for the charged cavity, most monomers assemble near the shell because of the attraction between the chain and the surface charges. Additionally, the monomer density has a long tail without oscillations. The counterions are depleted in the region near the density peak and the shell for the charged cavity [see Fig. 7(b)], as in the case of the charged capsid with smaller radius [Fig. 6(d)]. Nevertheless, for the neutral cavity the counterions are not depleted in the layer of monomers close to the surface [Fig. 7(a)]. The surface layer is less compact, because the monomer density is smaller.

To understand how the dynamics of counterion intrusion into the cavity is correlated with semiflexible polyelectrolyte packaging, we plot in Figure 8 the time evolution of the number of counterions which are adsorbed into the cavity. For the charged cavity, the dynamic change of the distribution of the negatively charged counterions (needed to balance the charges of the inner shell) is not shown because

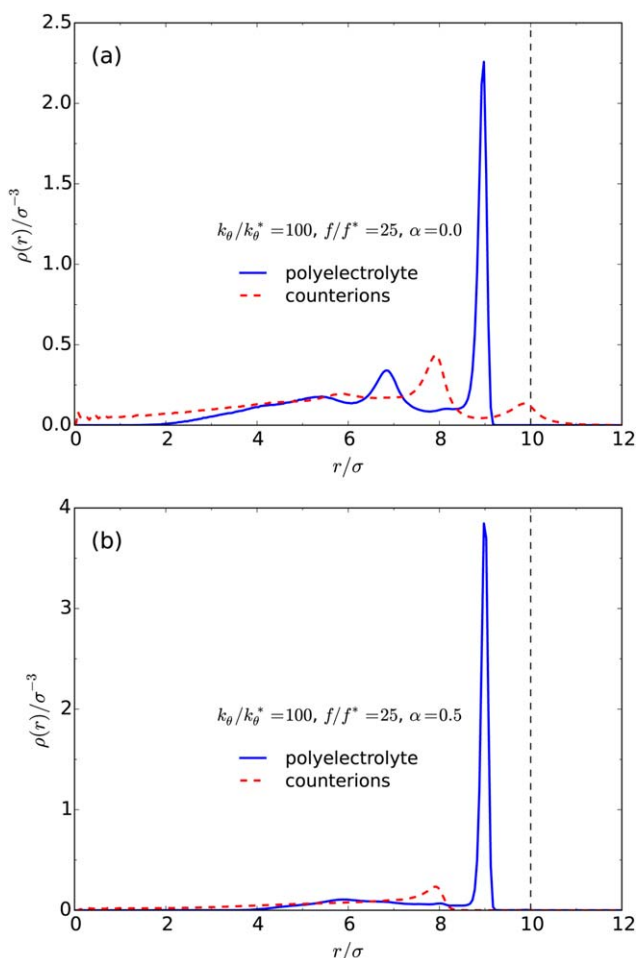


FIGURE 7 Radial density profiles of monomers and counterions as a function of the distance from the center of the cavity with radius $R = 10\sigma$. The vertical line represents the location of the inner shell. [Color figure can be viewed in the online issue, which is available at wileyonlinelibrary.com.]

these ions are mainly located outside the shell and exhausted rapidly during the packaging process. As the packaging process of the polyelectrolyte continues, the positive counterions are pulled into the cavity. If the inner shell of the cavity is neutral, not all counterions are adsorbed into the cavity, or the charges of polyelectrolyte are partially compensated. After the equilibrium state is reached, about 50% of the positive counterions are found in the cavity. The other counterions diffuse freely in the simulation box. Though the packaging process of the chain has pauses, there are no noteworthy delays in the adsorption process of the counterions. For the charged cavity, the packaging of the chain is much faster compared to the counterions. After the chain has been packaged, the counterions still need a long time to reach equilibrium in the cavity. Eventually, the charges of the packed polyelectrolyte are partially compensated by the adsorbed counterions and the charged shell.

After we have discussed the effects of electrostatic interactions and the impact of the motor force, we now investigate

the influence of the capsid radius upon the packaging dynamics of semiflexible polymers. In simulations with charged cavities, we kept the total number of surface charges constant at $N_c = 628$ and varied the capsid radius. Therefore, the surface charge density α is larger in a smaller cavity. The motor force was set to $f = 25f^*$. As it can be seen clearly in Figure 9, where the fraction of successfully packaged monomers is plotted as a function of time, the chain cannot fully be inserted if the cavity is too small (although it is in principle large enough to comfortably accommodate all monomers inside) and if the motor is too weak. This is so even if the surface charge density is maximal ($\alpha = 1$). In this case the packaging process is very fast initially until all surface charges are shielded by the surface layer of the polymer conformation. When the packaging density exceeds a certain value, where the drag force from surface charges is counterbalanced by the internal resistive force, the subsequent packaging is mainly driven by the motor force. The process often

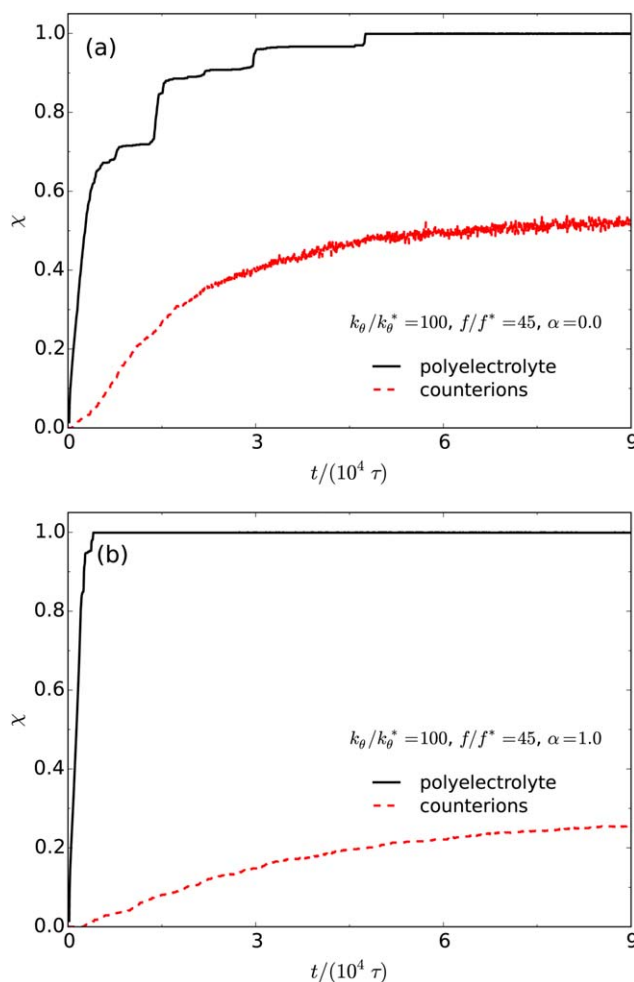


FIGURE 8 Time evolution of the packaging fraction χ of a semiflexible chain and its positively charged counterions in the absence and presence of surface charges. The motor force is fixed at $f = 45f^*$ and the cavity radius is $R = 7.07\sigma$. [Color figure can be viewed in the online issue, which is available at wileyonlinelibrary.com.]

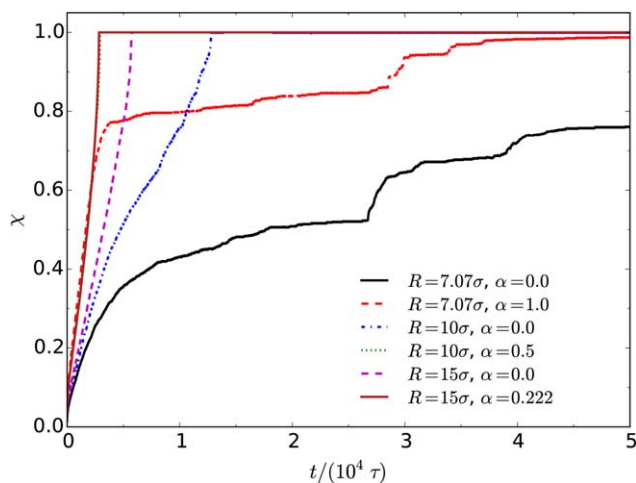


FIGURE 9 Time evolution of the packaging fraction χ of a semiflexible chain for different cavity radii in the absence ($\alpha=0$) and presence of surface charges ($\alpha>0$). The motor force is fixed at $f=25f^*$. For charged cavities, we set the number of surface charges to $N_c = 628$. As a result, $R = 7.07\sigma$, 10σ , and 15σ correspond to $\alpha = 1$, 0.5 , and 0.222 , respectively. [Color figure can be viewed in the online issue, which is available at wileyonlinelibrary.com.]

stalls because the motor force is comparatively weak. Packaging resumes after long pauses which are due to increased relaxation times of the polymer in the crowded space. The packaging of the entire chain into the cavity with radius $R = 7.07\sigma$ was neither accomplished in the case of the uncharged capsid nor when it was maximally charged.

For larger cavities we find that the packaging rate is not substantially affected by the cavity size if $R \geq 10\sigma$. Even if the capsid is uncharged, the polyelectrolyte is rapidly packaged.

We also discuss the time dependence of various energy components in the packaging process of the semiflexible chain for the charged cavity. Four different cases are shown in Figure 10. In the absence of motor force, the chain enters the cavity spontaneously to minimize the total potential energy E_{tot} [Fig. 10(a)]. Simultaneously, the total electrostatic energy E_{ele} is also reduced largely. In the packaging process, the intra-chain electrostatic repulsion E_{pp} enhances significantly. Compared to the electrostatic repulsion, the bending energy E_{ang} of the chain increases slowly. Therefore, the resistance of the intrusion of the polyelectrolyte in the cavity originates from the electrostatic interaction between charged monomers. However, the inherent bond rigidity plays an important role in controlling the ordered assembly of the chain

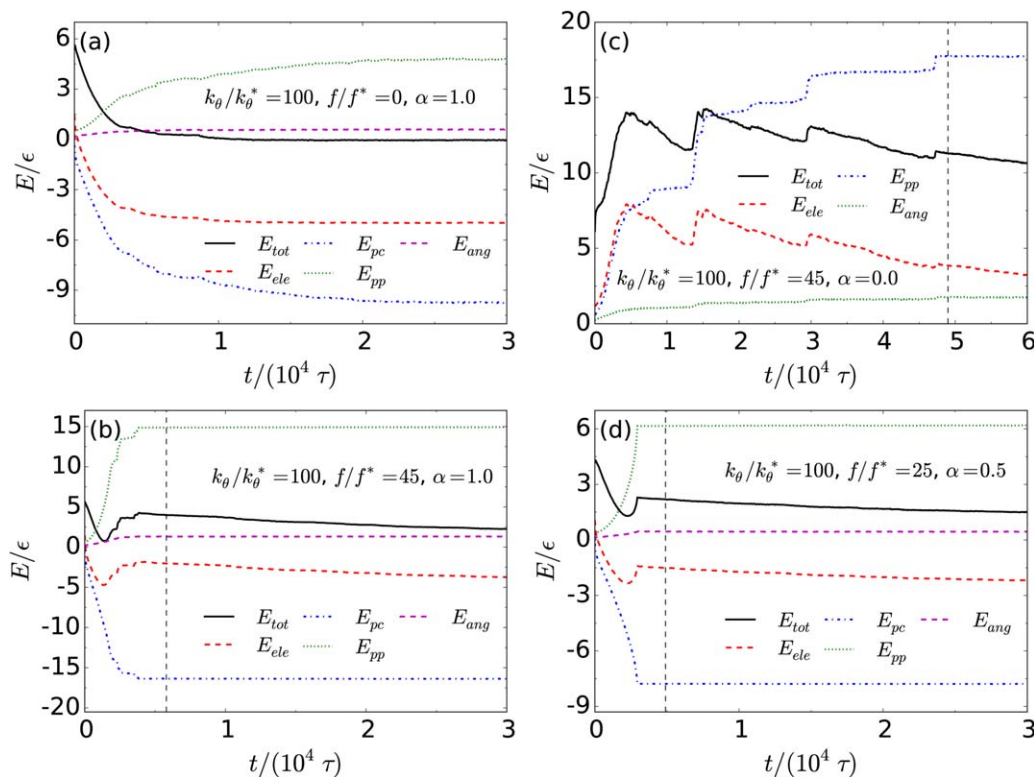


FIGURE 10 Different energy components of the semiflexible polymer as a function of simulation time. Shown are the total potential energy E_{tot} , total electrostatic energy E_{ele} , electrostatic energy E_{pc} between polyelectrolyte and cavity, bending energy E_{ang} of the polyelectrolyte, and electrostatic energy E_{pp} between monomers. In (a–c), the radius of cavity is $R = 7.07\sigma$, and (d) corresponds to $R = 10\sigma$. The vertical line represents the end time of packaging. [Color figure can be viewed in the online issue, which is available at wileyonlinelibrary.com.]

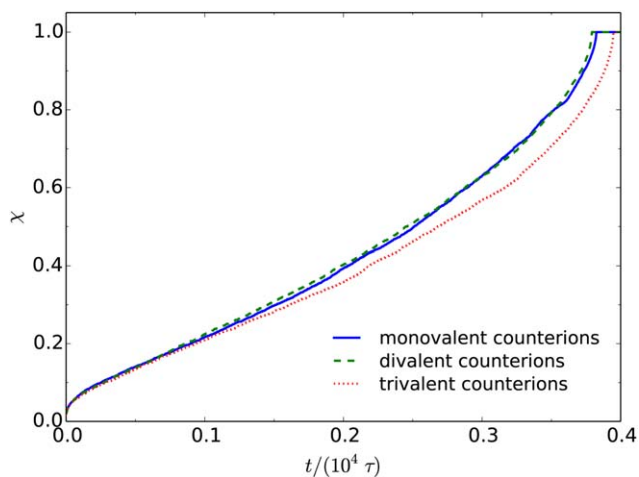


FIGURE 11 Time evolution of the packaging fraction χ of semiflexible chains in a capsid with radius $R = 10\sigma$ at $f = 25f^*$ and $\alpha = 0.5$. Three simulations for polyelectrolyte counterions with different valences were performed. [Color figure can be viewed in the online issue, which is available at wileyonlinelibrary.com.]

morphology. The electrostatic attraction E_{pc} between the chain and the charged shell is the main driving force of the packaging. The attraction energy decreases more rapidly, which is highly resistant to the repulsive interaction between monomers and the rigidity of the chain when the amount of charges of packaged chain segments is in proximity to that of the charged particles in the cavity. At a late stage of the packaging, most cavity charges are screened by the packaged monomers. Aided by the motor force, the packaging process is accelerated, and the remaining chain tail which cannot be pulled into the cavity in the absence of motor force is packed in the cavity. As shown in Figure 10(b), E_{tot} and E_{ele} decrease first, and then increase, accompanied by some pauses. After the packaging finishes, a slow decrease is attributed to aggregation of polyelectrolyte counterions.

If the inner shell of the cavity is uncharged, the packaging can only progress with the help of the motor. In the initial stage, all energetic components increase [see Fig. 10(c)]. It was found that E_{tot} and E_{ele} exhibit a sawtooth-like shape. The period of decreasing profiles of E_{tot} and E_{ele} corresponds to a pause in the packaging process, where the chain adjusts its conformation to lower free energy and counterions are adsorbed into the cavity. Electrostatic repulsion E_{pp} and bending energy E_{ang} are stepped up, which is consistent with the behavior of the packaging fraction of the chain. For the larger cavity, such as $R = 10\sigma$ [Fig. 10(d)], the change of the energy is similar to that for the smaller cavity [Fig. 10(b)], but the magnitude of change is smaller due to reduced curvature. For example, the intra-chain electrostatic energy is about 6ϵ , which is much lower compared to the cavity with $R = 7.07\sigma$, in which case it is about 15ϵ .

Multivalent ions have stronger binding ability to the polyelectrolyte compared to monovalent counterions, which tends to collapse the chain.⁴⁸ The effect of ionic valence on the

packing dynamics of viral genome is complicated, because ions not only affect the physics of genome confinement but also motor function.⁴⁹ In the present work, the interaction between motor and counterions is not considered. We present the packaging fraction versus time for different counterion valences in Figure 11. There is no evident difference in the packaging fraction for monovalent and divalent counterions under the parameters investigated. However, the intrusion process is delayed if trivalent counterions are present. Counterions with higher valence are strongly bound to the polyelectrolyte, which can suppress the electrostatic attraction between the polyelectrolyte and cavity to a certain extent. In the presence of the motor, the binding energy for low-valent counterions, such as monovalent and divalent ions, is not enough to counterbalance the motor force. In the initial stage, there is almost no discrepancy in the packaging profiles. This indicates that compared to the binding energy, strong electrostatic attraction between the polyelectrolyte and surface charges as well as low filling are dominant. Experimentally, there is no simple trend of the dependence on the packaging rate on capsid filling with changing ionic strength and valence due to the fact that ions influence the motor function. Nevertheless, it was observed that trivalent cations can screen DNA charges effectively.⁴⁹ In our work, a higher packaging velocity for trivalent counterions is identified in the final stage due to a collection of counterions in the cavity, leading to reduced internal force (see Fig. 12), which is consistent with mentioned experimental results.

We also calculate the charge proportion of condensed counterions and polyelectrolyte chain confined in the cavity for different counterion valences. The values for monovalent, divalent and trivalent counterions are 0.25, 0.31, and 0.34, respectively. In experiments on DNA condensation confined to two-dimensional cationic surfaces,⁵⁰ the charge proportion for divalent counterions is about 0.63 above critical salt concentration. At very low concentration, it is below 0.2. Our

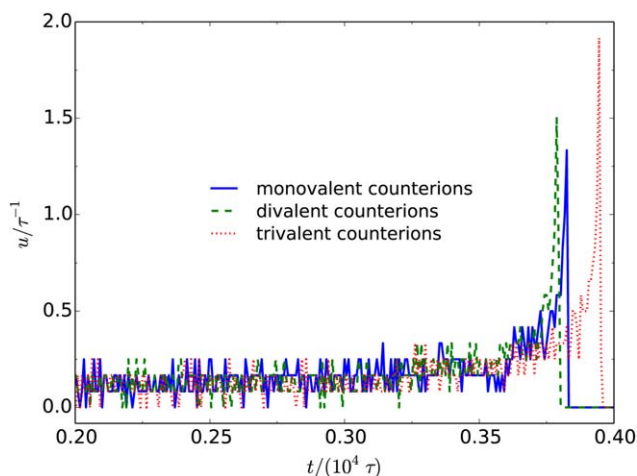


FIGURE 12 Packaging velocity of the polyelectrolyte for the same simulation parameters as in Figure 11. [Color figure can be viewed in the online issue, which is available at wileyonlinelibrary.com.]

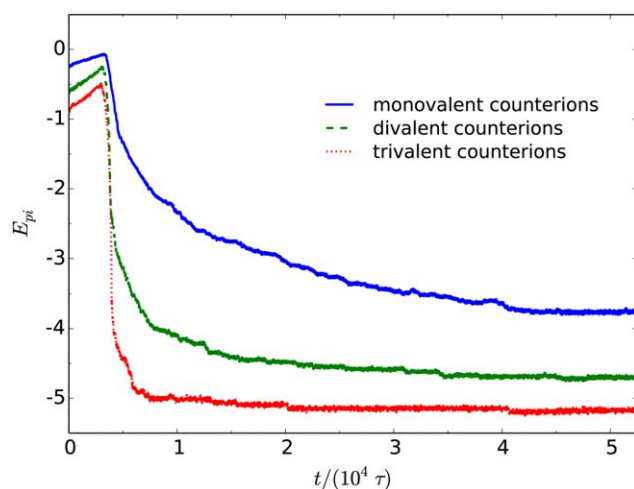


FIGURE 13 Electrostatic binding energy of counterions to polyelectrolyte chains as a function of simulation time. The parameters are same as those in Figure 11. [Color figure can be viewed in the online issue, which is available at wileyonlinelibrary.com.]

value for divalent counterions is in the range of experimental data.

Finally, we present the time evolution of the electrostatic binding energy E_{pi} of counterions to polyelectrolyte chains for different ionic valence in Figure 13. In the initial packaging process, the binding energy increases slowly because the counterions are separated from the chain. Then, an abrupt decrease was observed, when the total charges exceed the surface charges on the cavity surface, the counterions condense inside the cavity. Obviously, the binding energy for trivalent counterions drops more rapidly. It results in reduced internal forces or higher packaging velocity as discussed above.

CONCLUSIONS

We have investigated the packaging dynamics of flexible and semiflexible polyelectrolyte chains with 900 monomers in cavities, resembling viral capsids, under various conditions. For this purpose, extensive Langevin molecular dynamics simulations of a coarse-grained polyelectrolyte–capsid model were performed. By studying the influence of internal surface charge density, portal motor force, and cavity radius, we find that these parameters have to be well-tuned in order to enable the successful insertion of the polyelectrolyte into the capsid. Our virus model with ideal spherical shape is based on coarse-grained representation. Moreover, the present work does not specifically aim at explaining a single type of virus. Therefore, it is difficult to make some quantitative comparisons with experimental data. Only qualitative conclusions can be obtained at this point. However, we attempt some qualitative comparisons with available experimental results which are in good agreement with our simulations.

Surface charges located on the inner shell accelerate the packaging in the initial stage. Additionally, the presence of

surface charges supports the ordered arrangement of the first section of the chain in a surface layer. This affects a large number of monomers and the systematic covering of the interior capsid surface enables an optimal space filling by the subsequently intruding monomers. As a result, more additional inner space makes subsequent packaging easier. After the attraction of surface charges is counterbalanced by the internal resistance due to the reduced number of conformational states and the enhanced intrachain repulsion, the insertion of additional monomers is mainly driven by the motor force, especially for small cavities and low surface charge densities. If no motor force is present, a spring-like release of monomers off the cavity can occur.

Packaging a semiflexible chain was found to not necessarily take much longer than accommodating a flexible chain, when the surface charge density of capsid and the motor force are well balanced and enable to inject the chain into the capsid in a cooperative manner. Packed conformations of semiflexible chains which adopt ordered, layered spool-like structures, are more regular compared to those of flexible ones. Surface charges only are not sufficient to enable a smooth and efficient intrusion for the rather long chain. Not surprisingly, on the contrary, sufficiently large motor forces can “drive” the chain into the capsid without support by surface charges. The present work also addresses the effect of counterion valence on packaging dynamics and ionic binding energy. Regardless of the influence of ionic valence on motor function, the packaging process for trivalent counterions is delayed compared to lower-valent counterions. However, during the late stage of the packaging process it is accelerated for counterions with high valence. This is triggered by reduced intrachain repulsion due to the condensation of counterions into the cavity. The intrachain repulsion in the cavity is restrained conspicuously with increasing counterion valence, which is consistent with the prediction of viral DNA packaging experiments.⁴⁹

In our qualitative study structural details of the capsid were not taken into account. In ongoing studies, we explore the effects of local details of the inner shell, such as explicitly modeling peptide arms fixed to viral capsid, on the packaging dynamics.

ACKNOWLEDGMENTS

This work is supported by the NSF under Grant Nos. DMR-1207437 and DMR-1463241, National Natural Science Foundation of China under Grant No. 31500801, and by CNPq (National Council for Scientific and Technological Development, Brazil) under Grant No. 402091/2012-4. QC gratefully acknowledges support by the Alexander von Humboldt Foundation.

REFERENCES AND NOTES

- 1 J. Lidmar, L. Mirny, D. R. Nelson, *Phys. Rev. E* **2003**, *68*, 051910.

- 2 M. E. Cerritelli, N. Q. Cheng, A. H. Rosenberg, C. E. McPherson, F. P. Booy, A. C. Steven, *Cell* **1997**, *91*, 271.
- 3 W. Jiang, J. Chang, J. Jakana, P. Weigele, J. King, W. Chiu, *Nature* **2006**, *439*, 612.
- 4 Y. Z. Tao, N. H. Olson, W. Xu, D. L. Anderson, M. G. Rossmann, T. S. Baker, *Cell* **1998**, *95*, 431.
- 5 A. Fokine, P. R. Chipman, P. G. Leiman, V. V. Mesyanzhinov, V. B. Rao, M. G. Rossmann, *Proc. Natl. Acad. Sci. USA* **2004**, *101*, 6003.
- 6 Q. Q. Cao, M. Bachmann, *Phys. Rev. E* **2014**, *90*, 060601(R).
- 7 S. C. Harvey, A. S. Petrov, B. Devkota, M. B. Boz, *Phys. Chem. Chem. Phys.* **2009**, *11*, 10553.
- 8 J. Rong, Z. Niu, L. A. Lee, Q. Wang, *Curr. Opin. Colloid Interface Sci.* **2011**, *16*, 441.
- 9 T. Douglas, M. Young, *Science* **2006**, *312*, 873.
- 10 C. Chen, M.-C. Daniel, Z. T. Quinkert, M. De, B. Stein, V. D. Bowman, P. R. Chipman, V. M. Rotello, C. C. Kao, B. Dragnea, *Nano Lett.* **2006**, *6*, 611.
- 11 Y. J. Lee, H. Yi, W.-J. Kim, K. Kang, D. S. Yun, M. S. Strano, G. Ceder, A. M. Belcher, *Science* **2009**, *324*, 1051.
- 12 Y.-L. Loo, R. A. Register, A. J. Ryan, *Phys. Rev. Lett.* **2000**, *84*, 4120.
- 13 H. Arkin, W. Janke, *J. Phys. Chem. B* **2012**, *116*, 10379.
- 14 H. Arkin, W. Janke, *Phys. Rev. E* **2012**, *85*, 051802.
- 15 B. Hornblower, A. Coombs, R. D. Whitaker, A. Kolomeisky, S. J. Picone, A. Meller, M. Akeson, *Nat. Methods* **2007**, *4*, 315.
- 16 G. F. Schneider, C. Dekker, *Nat. Biotechnol.* **2012**, *30*, 326.
- 17 D. E. Smith, S. J. Tans, S. B. Smith, S. Grimes, D. L. Anderson, C. Bustamante, *Nature* **2001**, *413*, 748.
- 18 J. Kindt, S. Tzliil, A. Ben-Shaul, W. M. Gelbart, *Proc. Natl. Acad. Sci. USA* **2001**, *98*, 13671.
- 19 I. Ali, D. Marenduzzo, J. M. Yeomans, *Phys. Rev. Lett.* **2006**, *96*, 208102.
- 20 C. Forrey, M. Muthukumar, *Biophys. J.* **2006**, *91*, 25.
- 21 A. S. Petrov, S. C. Harvey, *Structure* **2007**, *15*, 21.
- 22 A. S. Petrov, M. B. Boz, S. C. Harvey, *J. Struct. Biol.* **2007**, *160*, 241.
- 23 K. Zhang, K. Luo, *J. Chem. Phys.* **2012**, *136*, 185103.
- 24 I. Ali, D. Marenduzzo, J. M. Yeomans, *J. Chem. Phys.* **2004**, *121*, 8635.
- 25 A. S. Petrov, C. R. Locker, S. C. Harvey, *Phys. Rev. E* **2009**, *80*, 021914.
- 26 I. Ali, D. Marenduzzo, *J. Chem. Phys.* **2011**, *135*, 095101.
- 27 A. S. Petrov, S. C. Harvey, *J. Struct. Biol.* **2011**, *174*, 137.
- 28 N. Stoop, J. Najafi, F. K. Wittel, M. Habibi, H. J. Herrmann, *Phys. Rev. Lett.* **2011**, *106*, 214102.
- 29 D. G. Angelescu, R. Bruinsma, P. Linse, *Phys. Rev. E* **2006**, *73*, 041921.
- 30 J. C. LaMarque, T.-V. L. Le, S. C. Harvey, *Biopolymers* **2004**, *73*, 348.
- 31 C. Forrey, M. Muthukumar, *J. Chem. Phys.* **2009**, *131*, 105101.
- 32 V. A. Belyi, M. Muthukumar, *Proc. Natl. Acad. Sci. USA* **2006**, *103*, 17174.
- 33 C. L. Ting, J. Wu, Z.-G. Wang, *Proc. Natl. Acad. Sci. USA* **2011**, *108*, 16986.
- 34 A. D. Migliori, N. Keller, T. I. Alam, M. Mahalingam, V. B. Rao, G. Arya, D. E. Smith, *Nat. Commun.* **2014**, *5*, 4173.
- 35 J. D. Perlmutter, C. Qiao, M. F. Hagan, *eLife* **2013**, *2*, e00632.
- 36 D. Marenduzzo, C. Micheletti, E. Orlandini, D. W. Sumners, *Proc. Natl. Acad. Sci. USA* **2013**, *110*, 20081.
- 37 R. Matthews, A. A. Louis, J. M. Yeomans, *Phys. Rev. Lett.* **2009**, *102*, 088101.
- 38 P. L. Freddolino, A. S. Arkhipov, S. B. Larson, A. McPherson, K. Schulten, *Structure* **2006**, *14*, 437.
- 39 Q. Q. Cao, M. Bachmann, *Soft Matter* **2013**, *9*, 5087.
- 40 M. Bachmann, *Thermodynamics and Statistical Mechanics of Macromolecular Systems*; Cambridge University Press, Cambridge **2014**.
- 41 Q. Q. Cao, C. C. Zuo, L. J. Li, Y. H. Ma, N. Li, *Microfluid. Nanofluid.* **2010**, *9*, 1051.
- 42 K. Kremer, G. S. Grest, *J. Chem. Phys.* **1990**, *92*, 5057.
- 43 R. W. Hockney, J. W. Eastwood, *Computer Simulation Using Particles*; Adam Hilger, Bristol, **1988**.
- 44 S. Plimpton, *J. Comp. Phys.* **1995**, *117*, 1.
- 45 G. S. Grest, K. Kremer, *Phys. Rev. A* **1986**, *33*, 3628.
- 46 O. V. Krasilnikov, C. G. Rodrigues, S. M. Bezrukov, *Phys. Rev. Lett.* **2006**, *97*, 018301.
- 47 M. Tihova, K. Dryden, T. Le, S. Harvey, J. Johnson, M. Yeager, A. Schneemann, *J. Virol.* **2004**, *7878*, 2897.
- 48 Q. Q. Cao, C. C. Zuo, H. W. He, L. J. Li, *Macromol. Theory Simulat.* **2009**, *18*, 441.
- 49 D. N. Fuller, J. P. Rickgauer, P. J. Jardine, S. Grimes, D. L. Anderson, D. E. Smith, *Proc. Natl. Acad. Sci. USA* **2007**, *104*, 11245.
- 50 I. Koltover, K. Wagner, C. R. Safinya, *Proc. Natl. Acad. Sci. USA* **2000**, *97*, 14046.